Experimental demonstration of quantum contextuality with nine observables on a single photonic qutrit

Xiao-Xiao Chen, Jian Li, Mairikena Aili, Zhe Meng, Ya-Jing Wang, and An-Ning Zhang[*]

Center for Quantum Technology Research and Key Laboratory of Advanced Optoelectronic Quantum Architecture and Measurements (MOE), School of Physics, Beijing Institute of Technology, Haidian District, Beijing 100081, People's Republic of China

The violation of contextuality inequalities shows a strong conflict between the noncontextual hidden variable theory and quantum mechanics. A single qutrit is the simplest indivisible quantum system that can allow a state-dependent contextuality test with five observables and a state-independent contextuality test with 13 observables. For any qutrit states, except for the maximally mixed state, one can always find a set of nine observables for which the corresponding inequality is violated [P. Kurzynski and D. Kaszlikowski, Phys. Rev. A **86**, 042125 (2012)]. In this paper, we demonstrate the violation of this inequality using single-photon experiments. Our experiments not only enrich the tests of quantum contextuality, but also deepen the understanding of the physical nature of quantum mechanics.

I. INTRODUCTION

The Kochen-Specker (KS) theorem [1,2] is the core of the foundation of quantum mechanics, which points out the conflict between the noncontextual hidden variable (NCHV) model and quantum theory. This conflict is generally referred to as quantum contextuality, i.e., the impossibility of assigning context-independent measurement outcomes that are in agreement with quantum predictions. The KS theorem was originally designed as a logical impossibility proof for value assignments and did not involve any statistical argument. This stimulated the development of a statistical version of the KS contradiction, so-called contextuality inequalities. This class of inequalities provides bounds that the NCHV model obey, similar to the bounds that Bell inequalities [3,4] provide for the local hidden variable model. Thus under some assumptions, contextuality tests can be achieved by the violation of contextuality inequalities [5,6].

The most basic examples of contextuality tests include the Klyachko-Can-Binicioglu-Shumovsky (KCBS) inequality and the Yu-Oh inequality. On the one hand, the KCBS inequality is the simplest inequality in a three-level system that includes only five observables, and it is a class of state-dependent contextuality tests [7]. Early experimental verifications of the KCBS inequality using a qutrit, the simplest system for testing quantum contextuality, were accomplished via a single photon [8,9]. Then more experimental verifications of the KCBS inequality were implemented in other quantum systems, such as trapped ion systems [10,11], superconducting systems [12], etc. On the other hand, Yu and Oh derived a greatly simplified state-independent contextuality test for qutrits, which involves 13 observables [13]. The experimental verification of the Yu-Oh inequality was also first implemented in a single photonic qutrit system [14]. Subsequently, further theoretical optimizations [15,16] and experimental verifications [17,18] of the Yu-Oh inequality were implemented. Interestingly, there is another Kurzynski-Kaszlikowski (KK) inequality [19] that is different from the KCBS and Yu-Oh inequalities, which can be violated by almost all states except for the maximally mixed state, thus allowing a contextuality test on the boundary between state dependent and state independent. The test of the KK inequality requires only nine observables to reveal the quantum contextuality for all qutrit states of a three-level system except for the maximally mixed state. Since this test lies on the boundary of state dependent and state independent, further research on it can help us to understand the relationship between the two types of contextuality tests to a certain extent. However, an experimental test of the KK inequality in quantum systems is lacking.

In this paper, we consider the theoretical scheme in Ref. [19] and experimentally demonstrate the violation of the KK inequality on a single photonic qutrit by introducing sequential measurements. We show that the KK inequality can be violated by two different qutrit states for the given nine observables in the theory. Our result agrees with the claim that given a qutrit state different from the maximally mixed one, one must correctly choose nine observables, and only then can the KK inequality be violated. We argue that the violation of the KK inequality is a third type of contextuality test distinct from state dependent and state independent, and it lies on the boundary between them. In other words, our work provides experimental proof of the contextuality test of the KK inequality in a photonic quantum system.

II. THEORETICAL SCHEME

Consider a qutrit and a set of nine two-outcome projectors $\Pi_i = |v_i\rangle\langle v_i|$, where $|v_i\rangle$ $(i = 1, 2, \ldots, 9)$ are the following

---

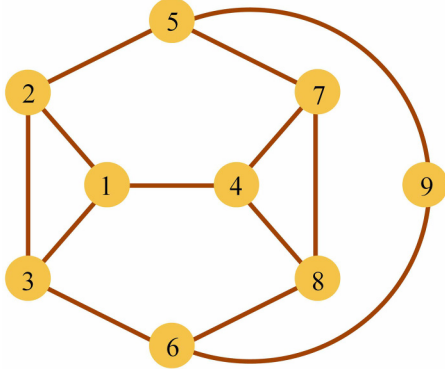[*]Corresponding author: anningzhang@bit.edu.cn

FIG. 1. The graph G of orthogonality relations among the nine vectors. The vectors are represented by vertices and the orthogonal vectors are connected by edges.

three-dimensional unit vectors [19]:

$$|v_1\rangle = (1, 0, 0)^T, \quad |v_2\rangle = (0, 1, 0)^T,$$

$$|v_3\rangle = (0, 0, 1)^T, \quad |v_4\rangle = \frac{1}{\sqrt{2}}(0, 1, -1)^T,$$

$$|v_5\rangle = \frac{1}{\sqrt{3}}(1, 0, -\sqrt{2})^T, \quad |v_6\rangle = \frac{1}{\sqrt{3}}(1, \sqrt{2}, 0)^T,$$

$$|v_7\rangle = \frac{1}{2}(\sqrt{2}, 1, 1)^T, \quad |v_8\rangle = \frac{1}{2}(\sqrt{2}, -1, -1)^T,$$

$$|v_9\rangle = \frac{1}{2}(\sqrt{2}, -1, 1)^T. \tag{1}$$

The orthogonality relationships among the nine vectors are presented in Fig. 1. For the nine projectors Π_i, their eigenvalues are 0 or 1. The orthogonality relations among Π_i follow from the orthogonality relations of the corresponding vectors $|v_i\rangle$, and are again summarized in the graph in Fig. 1. Moreover, the noncontextual bound was shown to be equal to the independence number $\mathcal{C}$ (it is the maximal number of mutually disjoined vertices in the graph) of the corresponding orthogonality graph G for the set of projectors Π_i [20]. Therefore, the independence number of the graph in Fig. 1 is 3 and the contextuality inequality derived in the theoretical scheme reads

$$\sum_{i=1}^{9} \langle \Pi_i \rangle \leqslant 3. \tag{2}$$

From the set of projectors Π_i listed in Fig. 1, one constructs the corresponding observables $A_i = 1 - 2\Pi_i$ whose eigenvalues are $+1$ or -1. The compatibility relations among the observables A_i follow from the orthogonality relations of the corresponding projectors Π_i. Substituting $A_i = 1 - 2\Pi_i$ into inequality (2), we obtain

$$\sum_{i=1}^{9} \langle A_i \rangle \geqslant 3. \tag{3}$$

Considering two compatible observables A_i and A_j, one can thus write the following contextuality inequality that is an equivalent form of inequality (2),

$$\sum_{(i,j)\in E(G)} \langle A_i A_j \rangle + \langle A_9 \rangle \geqslant -4. \tag{4}$$
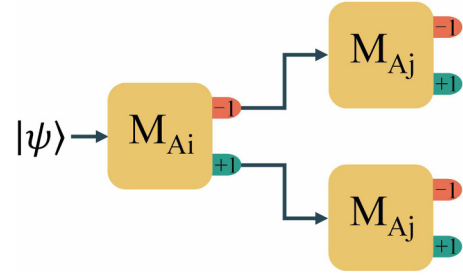

FIG. 2. Schematic of the sequential measurement device for two compatible observables $\langle A_i A_j \rangle$.

It is the so-called KK inequality, where $E(G)$ is the edge set of graph G which describes the compatibility relations of the nine observables. Inequalities (2) and (3) represent contextuality inequalities in terms of a set of nine single projectors and observables, respectively, while inequality (4) represents the contextuality inequality based on a set of two compatibility observables defined in the graph G. The violation of these inequalities indicates the contextual nature of a single qutrit state, although there is no unique set of nine measurements that tests the contextuality nature of every single qutrit state. According to theoretical predictions, for any qutrit states, except for the maximally mixed state, the corresponding inequalities can be violated as long as one chooses a set of nine vectors properly. Thus, taking a given set of nine vectors (1) as an example, we next experimentally verify the violation of inequalities (4) and (3) for some qutrit states.

III. EXPERIMENTAL DEMONSTRATION AND RESULTS

We now demonstrate the experimental test of the KK inequality using a single photonic qutrit system. In order to meet the requirements of the experimental test for contextuality, we measure the two compatible observables $\langle A_i A_j \rangle$ using sequential measurements [17,21,22]. Figure 2 is a schematic of the sequential measurement device for two compatible observables of the same photon. M_{A_i} and M_{A_j} denote the measurement devices for a single observable A_i and A_j, respectively. An arbitrary single photonic qutrit is prepared as the input state $|\psi\rangle$, and the photon first enters the measurement device M_{A_i} of A_i and produces one of two possible outcomes. Then, the photon enters the measurement device M_{A_j} of A_j and is finally detected in one of the output ports.

In the experiment, we use the polarization and path degrees of freedom of a single photon to prepare arbitrary qutrit states. The single photonic qutrit system always consists of one photon with two paths. The basis for our qutrit is encoded as $\{|0\rangle = |UH\rangle, |1\rangle = |LH\rangle, |2\rangle = |LV\rangle\}$, where U (L) denotes the upper (lower) path of single photons and $|H\rangle$ ($|V\rangle$) denotes their horizontal (vertical) polarizations. Our experimental setup includes the heralded single-photon source generation, qutrit state preparation, the observable measurements, and photon detection as illustrated in Fig. 3. As shown in Fig. 3(a), the photon pairs are generated from the spontaneous parametric down-conversion (SPDC) process in a type-II phase-matched periodically poled potassium titanyl phosphate (PPKTP) crystal. After the polarizing beam splitter
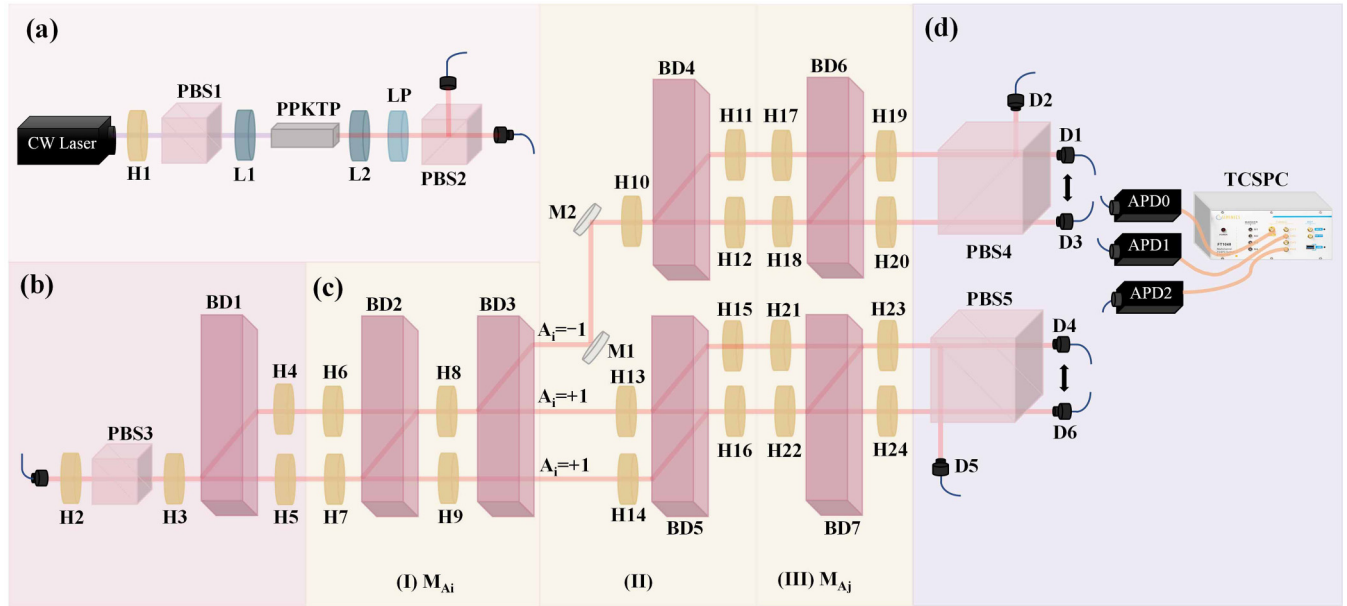
FIG. 3. Experimental setup. (a) Heralded single-photon source. A 405-nm continuous-wave (cw) diode laser with 20 mW power pumps a PPKTP crystal to produce photon pairs with a central wavelength of 810 nm based on SPDC. The H1 and PBS1 are used to regulate optical power. The two lenses (L1 and L2) are used for focusing and collimating beams. After filtering out the pumped laser with a LP, the photon pairs are split on PBS2 and are injected into APD0 and the optical network. (b) Qutrit state preparation. After the BD1, the photons are separated into the upper and lower paths depending on their polarizations, where the $|H\rangle$ ($|V\rangle$) polarization photons are in the upper (lower) paths. H3–H5(0°) are used to prepare $|\psi_1\rangle$, and H3(22.5°), H4(0°), and H5(45°) are used to prepare $|\psi_4\rangle$. (c) The observable measurements. This part includes three stages: (I) A_i measurement device M_{A_i}; (II) reconstruction of the corresponding eigenstate of A_i; (III) A_j measurement device M_{A_j}. (d) Photon detection. Photons from output ports D_{1-3} and D_{4-6} are detected using APD1 and APD2, respectively, whereas the heralding photons are detected by APD0. APD0, APD1, and APD2 are connected to a TCSPC. H, half-wave plate; PBS, polarizing beam splitter; LP, long-pass filter; BD, beam displacer; M, mirror; TCSPC, time-correlated single-photon counting.

2 (PBS2), one of the photons is directly detected by the single-photon avalanche photodiode (APD0) as a trigger, heralding that the other signal photon we use to test the inequality is prepared. In Fig. 3(b), the half-wave plate (HWP) H2 and PBS3 are used to regulate optical power and horizontal polarization. A beam displacer 1 (BD1) and H3–H5 are used to prepare the photonic three-level system in arbitrary desired qutrit states for testing. To show which qutrit states can violate inequalities (4) and (3) for a given set of nine vectors, we first perform theoretical simulations, and the results show that states $|\psi_1\rangle = |0\rangle$ and $|\psi_4\rangle = \frac{1}{\sqrt{2}}(|0\rangle + |1\rangle)$ can be violated (see Appendix A for details). So next our experiment shows the violation of inequalities (4) and (3) by the two qutrit states above.

As shown in Fig. 3(c), to measure the two compatible observables $\langle A_i A_j \rangle$, the setup in this part is divided into four stages. Stage (I) is the device M_{A_i} for A_i measurement. It includes four HWPs (H6–H9) and two BDs (BD2 and BD3). The angle settings of H6–H9 are chosen to project the eigenstate corresponding to $A_i = -1$ onto the $|H\rangle$ mode after BD3, whereas the other eigenstates with $A_i = +1$ are projected onto two $|V\rangle$ modes after BD3. Therefore there are three output ports of device M_{A_i} in the experiment. Before taking the M_{A_j} measurement, the eigenstates of $A_i = \pm 1$ need to be reconstructed, namely, stage (II). In the upper part of stage (II), the $A_i = -1$ mode is reprepared in its eigenstate with H10–H12 and BD4, while in the lower part of stage

(II), the $A_i = +1$ modes are reprepared with H13–H16 and BD5. Then we take the M_{A_j} measurement in stage (III). This stage consists of two identical A_j measurement devices M_{A_j} and each is connected to the corresponding output port of $A_i = \pm 1$. The upper (lower) device of M_{A_j} includes H17–H20 and BD6 (H21–H24 and BD7). The wave-plate angle settings are similar to device M_{A_i}, so there are a total of six output ports in the experiment. On the other hand, the setup for measuring a single observable A_i is the same as for measuring $A_i A_j$, but it will be simpler, because for all A_i, the angle settings of H10–H24 are the same except that the angle settings of H6–H9 are different. The purpose of this is simply to allow single photons to be detected by some specific detectors without any interferometers. The above angle settings of H6–H24 in the experiment setup for all measurements of the two input states are given in Appendix B.

Photons are detected by APDs that are connected with time-correlated single-photon counting (TCSPC), as shown in Fig. 3(d). We only record coincidence counts $C_{0,n}$ ($n = 1, \ldots, 6$) between APD1(2) and the trigger APD0 with a 2 ns coincidence time window, where APD1 and APD2 are connected with output ports D_{1-3} and D_{4-6}, respectively. For each measurement, we record clicks for 1 s, and register about 40 000 single photons. The probability for more than one photon pair is less than 10^{-6} and thus it can be neglected. After correcting the counts by the relative efficiencies of the different detectors, the coincidence counts are used

TABLE I. Experimental results of inequalities (4) and (3) for the two different input states being tested. The errors represent the statistical uncertainty obtained based on the Poissonian distribution assumption. Both of the inequalities are significantly violated by the experimental results.

Inequalities	Inequality (4)		Inequality (3)	
Input states	$\lvert\psi_1\rangle = \lvert 0\rangle$	$\lvert\psi_4\rangle = \frac{1}{\sqrt{2}}(\lvert 0\rangle + \lvert 1\rangle)$	$\lvert\psi_1\rangle = \lvert 0\rangle$	$\lvert\psi_4\rangle = \frac{1}{\sqrt{2}}(\lvert 0\rangle + \lvert 1\rangle)$
Experimental results	-5.0213 ± 0.0162	-5.0491 ± 0.0176	2.4873 ± 0.0113	2.5503 ± 0.0129
Theoretical predictions	-5.0002	-4.9570	2.6666	2.6810
$\sum_{i=1}^{9}(P_i - P_i')^2$	0.001 ± 0.0012		0.003 ± 0.0077	

to calculate the measured probabilities (see Appendix C for more experimental details). The measured probabilities are then used to calculate expectation values $\langle A_i A_j \rangle$ and $\langle A_i \rangle$ to evaluate the experimental results in inequalities (4) and (3).

In Table I, we present the measurement outcomes of these two inequalities (4) and (3) for two input states. For example, the experimental results -5.0213 ± 0.0162 and -5.0491 ± 0.0176 violate the contextuality bound of inequality (4) by 63 and 60 standard deviations and fit well with the theoretical predictions -5.0002 and -4.9570. We measure all 22 expectation values in inequalities (4) and (3) for two input states. Table II summarizes the experimental values and their theoretical predictions for the input state $\lvert\psi_4\rangle$. See Appendix D for the measurement results of the other input state. These results clearly violate the boundary set by the NCHV theory of inequalities (4) and (3).

IV. DISCUSSION AND CONCLUSION

The compatibility of measurements in contexts is an important issue in the experimental test of quantum contextuality [21]. Therefore, we also calculate the distance $\sum_{i=1}^{9}(P_i - P_i')^2$, where P_i is the measured probability of the observable A_i measured in one context and P_i' is the measured probability of the same observable measured in the other context. In Table I the results show the distances of both states tested are sufficiently small (<0.003), indicating that (almost) fully compatible measurements are achieved in our experiment.

In summary, we experimentally demonstrate a contextuality test of the KK inequalities (4) and (3) for a single photonic qutrit system. We observe that two single photonic qutrit states

not only violate inequality (4) involving compatible observables, but also inequality (3) involving single observables, although for any qutrit states, except for the maximally mixed state, one can always find a set of nine observables that reveal its contextuality using the KK inequalities (4) and (3). There is no unique set of nine measurements to test the contextuality of every qutrit state at present. In any case, our experiments realize the KK inequalities (4) and (3) in a photonic quantum system, which could open avenues for deeper experimental investigations.

APPENDIX A: THEORETICAL SIMULATIONS OF THE VIOLATION OF INEQUALITIES (4) AND (3)

As shown in Fig. 4, we perform theoretical simulations. The solid line represents the lower bound imposed by any noncontextual hidden variable (NCHV) model, while the dots represent the quantum mechanics (QM) prediction in the ideal input states. It is obvious that the maximally mixed state $\lvert\rho_8\rangle$ saturates both inequalities, that is, it satisfies their NCHV bounds. For a given set of vectors, having $\lvert\psi_1\rangle$ and $\lvert\psi_4\rangle$ can theoretically violate the two inequalities, as shown by the pink and dark blue regions in the bottom of Fig. 4.

APPENDIX B: THE ANGLE SETTINGS OF HWPS FOR $\langle A_i \rangle$ AND $\langle A_i A_j \rangle$

The details of the experimental setup for the measurements $\langle A_i \rangle$ and $\langle A_i A_j \rangle$ are shown in Table III.

TABLE II. Measured results of the 22 expectation values $\langle A_i \rangle$ and $\langle A_i A_j \rangle$ for the input state $\lvert\psi_4\rangle = \frac{1}{\sqrt{2}}(\lvert 0\rangle + \lvert 1\rangle)$.

| Observables	Experimental values	Theoretical predictions	Observables	Experimental values	Theoretical predictions
$\langle A_1 \rangle$	0.0157 ± 0.0024	0	$\langle A_1 A_4 \rangle$	-0.5175 ± 0.0045	-0.5
$\langle A_2 \rangle$	-0.0718 ± 0.0017	0	$\langle A_2 A_3 \rangle$	-0.0121 ± 0.0007	0
$\langle A_3 \rangle$	0.9792 ± 0.0055	1	$\langle A_2 A_5 \rangle$	-0.3283 ± 0.0031	-0.3333
$\langle A_4 \rangle$	0.4939 ± 0.0040	0.5	$\langle A_3 A_6 \rangle$	-0.9262 ± 0.0074	-0.9428
$\langle A_5 \rangle$	0.6438 ± 0.0045	0.6667	$\langle A_4 A_7 \rangle$	-0.9467 ± 0.0066	-0.9571
$\langle A_6 \rangle$	-0.9390 ± 0.0046	-0.9428	$\langle A_4 A_8 \rangle$	0.4516 ± 0.0053	0.4571
$\langle A_7 \rangle$	-0.4504 ± 0.0030	-0.4571	$\langle A_5 A_7 \rangle$	-0.7885 ± 0.0041	-0.7904
$\langle A_8 \rangle$	0.9387 ± 0.0056	0.9571	$\langle A_5 A_9 \rangle$	0.5734 ± 0.0034	0.6238
$\langle A_9 \rangle$	0.9402 ± 0.0055	0.9571	$\langle A_6 A_8 \rangle$	-0.9444 ± 0.0048	-0.9857
$\langle A_1 A_2 \rangle$	-0.9926 ± 0.0051	-1	$\langle A_6 A_9 \rangle$	-0.9437 ± 0.0048	-0.9857
$\langle A_1 A_3 \rangle$	-0.0634 ± 0.0018	0	$\langle A_7 A_8 \rangle$	-0.5509 ± 0.0041	-0.5
Inequality (4)	$\sum_{(i,j)}\langle A_i A_j \rangle + \langle A_9 \rangle = -5.0491 \pm 0.0176$		Inequality (3)	$\sum_{(i,j)}\langle A_i \rangle = 2.5503 \pm 0.0129$	
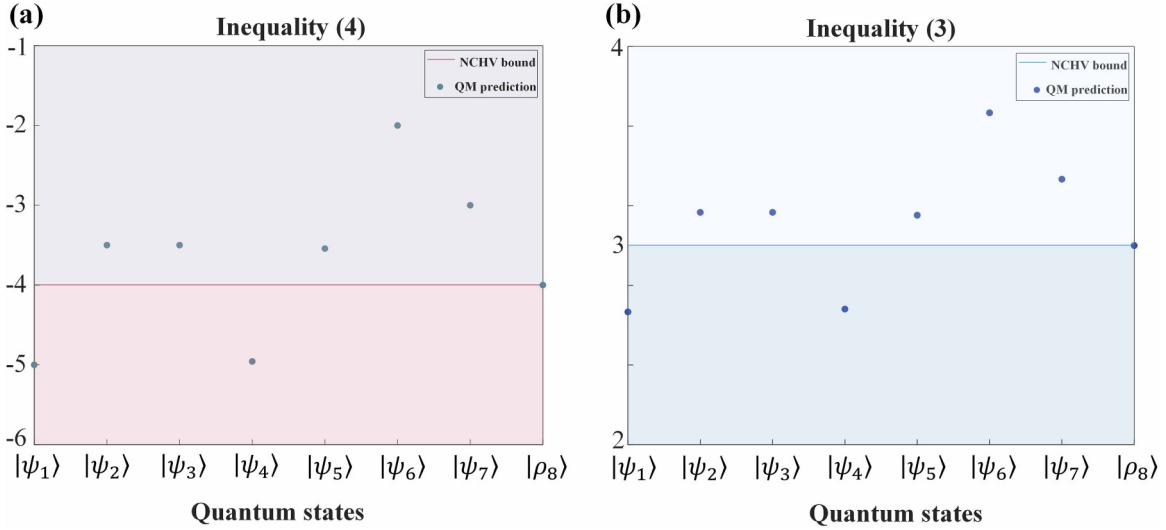
FIG. 4. Theoretical simulation for inequalities (4) [shown in (a)] and (3) [shown in (b)] under different input states. These input states are represented as $|\psi_1\rangle = |0\rangle$, $|\psi_2\rangle = |1\rangle$, $|\psi_3\rangle = |2\rangle$, $|\psi_4\rangle = \frac{1}{\sqrt{2}}(|0\rangle + |1\rangle)$, $|\psi_5\rangle = \frac{1}{\sqrt{2}}(|0\rangle + |2\rangle)$, $|\psi_6\rangle = \frac{1}{\sqrt{2}}(|1\rangle + |2\rangle)$, $|\psi_7\rangle = \frac{1}{\sqrt{3}}(|0\rangle + |1\rangle + |2\rangle)$, and $|\rho_8\rangle = \frac{1}{3}(|0\rangle\langle 0| + |1\rangle\langle 1| + |2\rangle\langle 2|)$.

APPENDIX C: EXPERIMENTAL DETAILS

In the experiment, before evaluating the measured probabilities of each measurement, we first estimate the relative detector efficiencies of each detector. This is done by making all the photons in APD1 and APD2 coincide by measuring with the trigger APD0, and recording the photon coincidence counts as n_1 and n_2, where APD1 and APD2 detect photons from outports D_{1-3} and D_{4-6}, respectively. The efficiency of

APD1 relative to APD2 is then

$$\eta_1 = \frac{n_1}{n_2}. \tag{C1}$$

When measuring $\langle A_i \rangle$, $C_{0,1-3}$ correspond to $A_i = -1$, and $C_{0,4-6}$ correspond to $A_i = +1$. However, when measuring $\langle A_i A_j \rangle$, $C_{0,1}$ corresponds to the event of $A_i = -1$ and $A_j = -1$; $C_{0,2}$ and $C_{0,3}$ correspond to $A_i = -1$ and $A_j = +1$;

TABLE III. Some HWPs are not listed in the table because they have the same angles in each measurement. These HWPs are H6(45°), H9(0°), H11(0°), H17(45°), H21(45°), and H24(0°).

HWP	H7	H8	H10	H12	H13	H14	H15	H16	H18	H19	H20	H22	H23
$\langle A_1 \rangle$	0°	45°	0°	0°	45°	0°	45°	0°	45°	0°	45°	0°	45°
$\langle A_2 \rangle$	0°	0°	0°	0°	45°	0°	45°	0°	45°	0°	45°	0°	45°
$\langle A_3 \rangle$	45°	0°	0°	0°	45°	0°	45°	0°	45°	0°	45°	0°	45°
$\langle A_4 \rangle$	22.5°	0°	0°	0°	45°	0°	45°	0°	45°	0°	45°	0°	45°
$\langle A_5 \rangle$	45°	72.4°	0°	0°	45°	0°	45°	0°	45°	0°	45°	0°	45°
$\langle A_6 \rangle$	0°	17.6°	0°	0°	45°	0°	45°	0°	45°	0°	45°	0°	45°
$\langle A_7 \rangle$	22.5°	22.5°	0°	0°	45°	0°	45°	0°	45°	0°	45°	0°	45°
$\langle A_8 \rangle$	22.5°	157.5°	0°	0°	45°	0°	45°	0°	45°	0°	45°	0°	45°
$\langle A_9 \rangle$	157.5°	157.5°	0°	0°	45°	0°	45°	0°	45°	0°	45°	0°	45°
$\langle A_1 A_2 \rangle$	0°	45°	0°	0°	0°	45°	0°	45°	0°	0°	0°	0°	0°
$\langle A_1 A_3 \rangle$	0°	45°	0°	0°	0°	45°	0°	45°	45°	0°	0°	45°	0°
$\langle A_1 A_4 \rangle$	0°	45°	0°	0°	0°	45°	0°	45°	22.5°	0°	0°	22.5°	0°
$\langle A_2 A_3 \rangle$	0°	0°	45°	45°	45°	45°	0°	45°	45°	0°	0°	45°	0°
$\langle A_2 A_5 \rangle$	0°	0°	45°	45°	45°	45°	0°	45°	45°	72.4°	0°	45°	72.4°
$\langle A_3 A_6 \rangle$	45°	0°	45°	0°	45°	45°	0°	0°	0°	17.6°	0°	0°	17.6°
$\langle A_4 A_7 \rangle$	22.5°	0°	45°	22.5°	45°	45°	0°	22.5°	22.5°	22.5°	0°	22.5°	22.5°
$\langle A_4 A_8 \rangle$	22.5°	0°	45°	22.5°	45°	45°	0°	22.5°	22.5°	157.5°	0°	22.5°	157.5°
$\langle A_5 A_7 \rangle$	45°	72.4°	27.4°	0°	27.4°	135°	0°	0°	22.5°	22.5°	0°	22.5°	22.5°
$\langle A_5 A_9 \rangle$	45°	72.4°	27.4°	0°	27.4°	135°	0°	0°	157.5°	157.5°	0°	157.5°	157.5°
$\langle A_6 A_8 \rangle$	0°	17.6°	27.4°	45°	27.4°	135°	0°	45°	22.5°	157.5°	0°	22.5°	157.5°
$\langle A_6 A_9 \rangle$	0°	17.6°	27.4°	45°	27.4°	135°	0°	45°	157.5°	157.5°	0°	157.5°	157.5°
$\langle A_7 A_8 \rangle$	22.5°	22.5°	157.5°	157.5°	157.5°	135°	0°	157.5°	22.5°	157.5°	0°	22.5°	157.5°

TABLE IV. Measured results of the 22 expectation values $\langle A_i \rangle$ and $\langle A_i A_j \rangle$ for the input state $|\psi_1\rangle = |0\rangle$.

Observables	Experimental values	Theoretical predictions	Observables	Experimental values	Theoretical predictions
$\langle A_1 \rangle$	-0.9955 ± 0.0036	-1	$\langle A_1 A_4 \rangle$	-0.9952 ± 0.0063	-1
$\langle A_2 \rangle$	0.9888 ± 0.0053	1	$\langle A_2 A_3 \rangle$	0.9978 ± 0.0052	1
$\langle A_3 \rangle$	0.9844 ± 0.0054	1	$\langle A_2 A_5 \rangle$	0.3194 ± 0.0032	0.3333
$\langle A_4 \rangle$	0.9816 ± 0.0052	1	$\langle A_3 A_6 \rangle$	0.3239 ± 0.0035	0.3333
$\langle A_5 \rangle$	0.3257 ± 0.0033	0.3333	$\langle A_4 A_7 \rangle$	0.0037 ± 0.0005	0
$\langle A_6 \rangle$	0.3305 ± 0.0034	0.3333	$\langle A_4 A_8 \rangle$	-0.0074 ± 0.0006	0
$\langle A_7 \rangle$	-0.0386 ± 0.0016	0	$\langle A_5 A_7 \rangle$	-0.6428 ± 0.0039	-0.6667
$\langle A_8 \rangle$	-0.0438 ± 0.0016	0	$\langle A_5 A_9 \rangle$	-0.6446 ± 0.0039	-0.6667
$\langle A_9 \rangle$	-0.0457 ± 0.0016	0	$\langle A_6 A_8 \rangle$	-0.6779 ± 0.0042	-0.6667
$\langle A_1 A_2 \rangle$	-0.9954 ± 0.0064	-1	$\langle A_6 A_9 \rangle$	-0.6761 ± 0.0042	-0.6667
$\langle A_1 A_3 \rangle$	-0.9932 ± 0.0064	-1	$\langle A_7 A_8 \rangle$	-0.9879 ± 0.0047	-1
Inequality (4)	$\sum_{(i,j)} \langle A_i A_j \rangle + \langle A_9 \rangle = -5.0213 \pm 0.0162$		Inequality (3)	$\sum_{(i,j)} \langle A_i \rangle = 2.4873 \pm 0.0113$	

$C_{0,4}$ corresponds to $A_i = +1$ and $A_j = -1$; $C_{0,5}$ and $C_{0,6}$ correspond to $A_i = +1$ and $A_j = +1$. Then, $\langle A_i \rangle$ and $\langle A_i A_j \rangle$ are calculated from

$$\langle A_i \rangle = P(A_i = +1) - P(A_i = -1), \tag{C2}$$

$$\langle A_i A_j \rangle = P(A_i = -1, A_j = -1) - P(A_i = -1, A_j = +1) \\ - P(A_i = +1, A_j = -1) + P(A_i = +1, A_j = +1). \tag{C3}$$

Here, $P(A_i = \pm 1, A_j = \pm 1)$ are the measured joint probability distributions of the corresponding compatible observables $A_i A_j$ and $P(A_i = \pm 1)$ are the probability distributions of the measure of the single observable A_i. These probability distributions can be calculated from the measured coincidence counts given as

$$P(A_i = -1) = \frac{C'_{0,1} + C'_{0,2} + C'_{0,3}}{C'_N},$$

$$P(A_i = +1) = \frac{C_{0,4} + C_{0,5} + C_{0,6}}{C'_N}. \tag{C4}$$

$$P(A_i = -1, A_j = -1) = \frac{C'_{0,1}}{C'_N},$$

$$P(A_i = -1, A_j = +1) = \frac{C'_{0,1} + C'_{0,2}}{C'_N},$$

$$P(A_i = +1, A_j = -1) = \frac{C_{0,4}}{C'_N}, \tag{C5}$$

$$P(A_i = +1, A_j = +1) = \frac{C_{0,5} + C_{0,6}}{C'_N},$$

where $C'_{0,1-3}$ are the corresponding coincidence counts for $C_{0,1-3}$ corrected by their relative photon collection efficiency η_1 and $C'_N = \sum_{n=1}^{3} C'_{0,n} + \sum_{n=4}^{6} C_{0,n}$ is the corrected total coincidence counts.

APPENDIX D: DETAILS OF EXPERIMENTAL RESULTS

The details of the measured results of the 22 expectation values $\langle A_i \rangle$ and $\langle A_i A_j \rangle$ for the input state $|\psi_1\rangle = |0\rangle$ are shown in Table IV.

[1] S. Kochen and E. P. Specker, The problem of hidden variables in quantum mechanics, J. Math. Mech. **17**, 59 (1967).

[2] J. S. Bell, On the problem of hidden variables in quantum mechanics, Rev. Mod. Phys. **38**, 447 (1966).

[3] J. S. Bell, On the Einstein Podolsky Rosen paradox, Phys. Phys. Fiz. **1**, 195 (1964).

[4] J. F. Clauser, M. A. Horne, A. Shimony, and R. A. Holt, Proposed Experiment to Test Local Hidden-Variable Theories, Phys. Rev. Lett. **23**, 880 (1969).

[5] C. Budroni, A. Cabello, O. Gühne, M. Kleinmann, and J. Å. Larsson, Kochen-Specker contextuality, Rev. Mod. Phys. **94**, 045007 (2022).

[6] J. Thompson, P. Kurzyński, S. Y. Lee, A. Soeda, and D. Kaszlikowski, Recent advances in contextuality tests, Open Syst. Inf. Dyn. **23**, 1650009 (2016).

[7] A. A. Klyachko, M. A. Can, S. Binicioğlu, and A. S. Shumovsky, Simple Test for Hidden Variables in Spin-1 Systems, Phys. Rev. Lett. **101**, 020403 (2008).

[8] R. Lapkiewicz, P. Li, C. Schaeff, N. K. Langford, S. Ramelow, M. Wieśniak, and A. Zeilinger, Experimental non-classicality of an indivisible quantum system, Nature (London) **474**, 490 (2011).

[9] J. Ahrens, E. Amselem, A. Cabello, and M. Bourennane, Two fundamental experimental tests of nonclassicality with qutrits, Sci. Rep. **3**, 2170 (2013).

[10] M. Um, X. Zhang, J. Zhang, Y. Wang, S. Yangchao, D.-L. Deng, L.-M. Duan, and K. Kim, Experimental certification of random numbers via quantum contextuality, Sci. Rep. **3**, 1627 (2013).

[11] M. Malinowski, C. Zhang, F. M. Leupold, A. Cabello, J. Alonso, and J. P. Home, Probing the limits of correlations in an indivisible quantum system, Phys. Rev. A **98**, 050102(R) (2018).

[12] M. Jerger, Y. Reshitnyk, M. Oppliger, A. Potočnik, M. Mondal, A. Wallraff, K. Goodenough, S. Wehner, K. Juliusson, N. K. Langford, and A. Fedorov, Contextuality without nonlocality in a superconducting quantum system, Nat. Commun. **7**, 12930 (2016).

[13] S. Yu and C. H. Oh, State-Independent Proof of Kochen-Specker Theorem with 13 Rays, Phys. Rev. Lett. **108**, 030402 (2012).

[14] C. Zu, Y. X. Wang, D. L. Deng, X. Y. Chang, K. Liu, P. Y. Hou, H. X. Yang, and L. M. Duan, State-Independent Experimental Test of Quantum Contextuality in an Indivisible System, Phys. Rev. Lett. **109**, 150401 (2012).

[15] A. Cabello, E. Amselem, K. Blanchfield, M. Bourennane, and I. Bengtsson, Proposed experiments of qutrit state-independent contextuality and two-qutrit contextuality-based nonlocality, Phys. Rev. A **85**, 032108 (2012).

[16] M. Kleinmann, C. Budroni, J. Å. Larsson, O. Gühne, and A. Cabello, Optimal Inequalities for State-Independent Contextuality, Phys. Rev. Lett. **109**, 250402 (2012).

[17] Y. F. Huang, M. Li, D. Y. Cao, C. Zhang, Y. S. Zhang, B. H. Liu, C. F. Li, and G. C. Guo, Experimental test of state-independent quantum contextuality of an indivisible quantum system, Phys. Rev. A **87**, 052133 (2013).

[18] F. M. Leupold, M. Malinowski, C. Zhang, V. Negnevitsky, A. Cabello, J. Alonso, and J. P. Home, Sustained State-Independent Quantum Contextual Correlations from a Single Ion, Phys. Rev. Lett. **120**, 180401 (2018).

[19] P. Kurzynski and D. Kaszlikowski, Contextuality of almost all qutrit states can be revealed with nine observables, Phys. Rev. A **86**, 042125 (2012).

[20] A. Cabello, S. Severini, and A. Winter, Graph-Theoretic Approach to Quantum Correlations, Phys. Rev. Lett. **112**, 040401 (2014).

[21] D. K. Qu, P. Kurzynski, D. Kaszlikowski, S. Raeisi, L. Xiao, K. K. Wang, X. Zhan, and P. Xue, Experimental entropic test of state-independent contextuality via single photons, Phys. Rev. A **101**, 060101(R) (2020).

[22] P. Xue, L. Xiao, G. Ruffolo, A. Mazzari, T. Temistocles, M. T. Cunha, and R. Rabelo, Synchronous Observation of Bell Nonlocality and State-Dependent Contextuality, Phys. Rev. Lett. **130**, 040201 (2023).